

1 **The Relationship Between Cloud Radiative Effect and**
2 **Surface Temperature Variability at ENSO Frequencies**
3 **in CMIP5 Models**

4 **Nicholas J. Lutsko¹**

5 ¹Department of Earth, Atmospheric, and Planetary Sciences, Massachusetts Institute of Technology,
6 Cambridge, Massachusetts

7 **Key Points:**

- 8 • Low clouds dominate the relationship between clouds and surface temperatures
9 at ENSO frequencies.
- 10 • This is due to the thermodynamic variability of low clouds and not to changes in
11 the large-scale dynamics.
- 12 • The cloud radiative effect due to low clouds during ENSO events is well correlated
13 with models' sensitivities.

Corresponding author: Nicholas Lutsko, lutsko@mit.edu

14 **Abstract**

15 The relationship between the tropical cloud radiative effect (CRE) and tropical sur-
16 face temperature variability on ENSO time-scales is investigated in pre-industrial con-
17 trol simulations from the CMIP5 archive. The tropical CRE is binned according to mid-
18 tropospheric vertical velocities and then regressed in frequency space versus tropical-mean
19 surface temperatures. Low clouds play a leading role in the relationship between clouds
20 and surface temperature variability, amplifying ENSO-induced surface temperature anoma-
21 lies through thermodynamically-driven changes in the short-wave CRE. Changes in CRE
22 driven by changes in the large-scale dynamics have a minor influence on surface temper-
23 ature variability. It is shown that the regression co-efficients at ENSO frequencies be-
24 tween the CRE in regions of moderate subsidence and of weak ascent, and tropical-mean
25 surface temperatures are well correlated with models' climate sensitivities, constituting
26 a potential "emergent constraint" on climate sensitivity.

27 **1 Introduction**

28 There is a well established connection between ENSO events and global-mean sur-
29 face temperature (GMST), with El Niño events causing an increase in GMST and La
30 Niña events causing a decrease. The changes in GMST are driven primarily by sea sur-
31 face temperature (SST) anomalies in the tropical Pacific, which warm or cool the entire
32 troposphere above them depending on the phase and amplitude of the ENSO event. These
33 signals are then rapidly communicated to other parts of the tropics, since the tropical
34 atmosphere cannot sustain large temperature gradients [*Sobel and Bretheron, 2000*]. The
35 warming or cooling of surface temperatures outside the tropical Pacific is more complex
36 however, as the strength of the coupling between SSTs and the free troposphere above
37 them has significant regional variations and so the surface temperatures of certain re-
38 gions in the Indian and Atlantic oceans are not well correlated with ENSO variability
39 [*Chiang and Sobel, 2002*].

40 Clouds also play a role in the response of GMST to ENSO events, and their net
41 effect on ENSO is determined by a complex interplay between reductions (increases) in
42 low cloud cover in regions of mean subsidence and increases (reductions) in convective
43 cloudiness in regions of mean ascent during El Niño (La Niña) events (e.g., *Klein and*
44 *Hartmann [1993]; Bony et al. [1997]; Park and Leovy [2004]; Radel et al. [2016]*), with

45 the former amplifying surface temperature variability and the latter reducing it. Because
46 the two effects partly cancel each other, it has proven difficult to untangle their relative
47 contributions, though *Lloyd et al.* [2012] showed that the low cloud effect is the primary
48 contributor to the difference between model feedbacks onto ENSO and those seen in ob-
49 servations.

50 Since low clouds are the source of much of the intermodel spread in Equilibrium
51 Climate Sensitivity (ECS; e.g., *Vial et al.* [2013]), it is tempting to use their ENSO-induced
52 variability to constrain their forced changes. However recent work has shown that cloud
53 feedbacks are highly sensitive to the pattern of surface temperature change (*Andrews et al.*
54 [2015]; *Zhou et al.* [2017]; *Silvers et al.* [2018]; *Andrews and Webb* [2018]), in particular
55 whether the warming is focused in regions of mean ascent or in regions of mean subsi-
56 dence, or in the extratropics. This is problematic for attempts to constrain forced changes
57 in clouds from ENSO-induced changes, as the patterns of low cloud changes during ENSO
58 events differ from what is seen in forced simulations (*Zhu et al.* [2007]). On the other
59 hand, there is statistical evidence that cloud feedbacks on unforced variability are related
60 to forced cloud feedbacks (*Zhou et al.* [2015]; *Brient and Schneider* [2016]; *Colman and*
61 *Hanson* [2017]), suggesting that ENSO-induced cloud changes could be used to infer how
62 clouds will change in a warmer world.

63 This study addresses these two questions – the relationships between different cloud
64 types and tropical surface temperatures, and whether cloud changes on ENSO time-scales
65 can be used to infer forced cloud changes – by applying two analysis techniques to data
66 from the pre-industrial control simulations in the fifth Climate Model Intercomparison
67 Project (CMIP5) archive. The first is binning the cloud radiative effect (CRE, defined
68 below) based on the pressure velocity at 500hPa (ω) of each grid point. This is a com-
69 monly used technique for assessing the contributions of different cloud types to forced
70 cloud changes in climate models (e.g., *Bony et al.* [2004]; *Bony and Dufresne* [2005]; *Wyant*
71 *et al.* [2006]; *Zhao et al.* [2016]; *Byrne and Schneider* [2018]), and here permits the con-
72 tribution of different cloud types to surface temperature variability on ENSO time-scales
73 to be quantified.

74 The second technique is frequency-dependent regressions, which *Lutsko and Taka-*
75 *hashi* [2018] used to study the relationship between TOA fluxes and surface tempera-
76 tures in data from the pre-industrial control simulations in the CMIP5 archive (see also

77 *MacMynowski et al.* [2011]). A frequency-dependent “sensitivity” can be defined for these
78 unforced simulations using the regression co-efficients between CRE and surface temper-
79 ature, and a strong correlation was found across models between these regression co-efficients
80 and the models’ ECS values on time-scales of 2.5 to 3 years. This constitutes a poten-
81 tial “emergent constraint” between the behavior of clouds on ENSO time-scales and mod-
82 els’ responses to increased CO₂ concentrations, though it was found that roughly 100
83 years of data are required for a strong relationship to emerge.

84 Besides the regression co-efficients, the frequency-dependent regressions also pro-
85 vide information about the relative phase of the CRE and surface temperature. Lutsko
86 and Takahashi found that, in the ensemble-median, the CRE is approximately 90° out
87 of phase with tropical surface temperatures on ENSO frequencies. Naively, this implies
88 that tropical clouds force surface temperature variability on these time-scales, but based
89 on previous studies of the relationship between clouds and tropical surface temperatures
90 on ENSO time-scales (*Klein et al.* [1999]; *Lau and Nath* [2001]; *Zhu et al.* [2007]; *Zhou*
91 *et al.* [2017]), it was suggested instead that tropical clouds rapidly respond to SST anoma-
92 lies in the equatorial Pacific and then amplify tropical-mean surface temperature anoma-
93 lies generated by the local SST anomalies during ENSO events.

94 Building on this work, the CRE in the pre-industrial control simulations is here de-
95 composed into ω bins and then regressed in frequency space versus tropical-mean sur-
96 face temperatures. This permits the relationships between different cloud types and trop-
97 ical surface temperatures to be investigated as a function of frequency, though the fo-
98 cus here is on ENSO time-scales (\sim 2-5 years). This decomposition can also be used to
99 identify which cloud-types are responsible for the relationship between the regression co-
100 efficients and the models’ sensitivities. A strong correlation across models is found be-
101 tween the changes in CRE due to clouds in regions of weak ascent and weak to moder-
102 ate subsidence on ENSO time-scales and the models’ ECS values, which constitutes a
103 stricter emergent constraint on Earth’s ECS than that proposed by Lutsko and Taka-
104 hashi.

105 After describing the data and methods used in the study in section 2, the relation-
106 ship between tropical-mean surface temperature variability and thermodynamic changes
107 in CRE (changes independent of changes in the large-scale dynamics) is investigated in
108 section 3, and then the relationship between tropical-mean surface temperature variabil-

109 ity and variability in CRE due to changes in the large-scale dynamics is investigated in
 110 section 4. Section 5 examines which cloud types are responsible for the relationship be-
 111 tween the regression co-efficients and the models' ECS values seen by Lutsko and Taka-
 112 hashi, before conclusions are drawn in section 6.

113 2 Data and Methods

114 2.1 Data

115 The analysis used monthly data from the pre-industrial control (“pi-control”) ex-
 116 periments with 18 models participating in the CMIP5 project (Supplementary Table 1).
 117 500 simulation years were used for each model and in cases where more than 500 years
 118 of data are available only the first 500 years were retained. The variables used in the anal-
 119 ysis were the vertical pressure velocity at 500hPa, surface air temperature, the SSTs, the
 120 TOA outgoing long-wave radiation, the TOA outgoing short-wave radiation, the TOA
 121 outgoing clear-sky long-wave radiation and the TOA outgoing clear-sky short-wave ra-
 122 diation. The incoming solar radiation was assumed to be fixed and the net CRE was com-
 123 puted as the net all-sky flux (long-wave + short-wave) minus the net clear-sky flux. Sim-
 124 ilarly, the short-wave (long-wave) CRE was computed as the all-sky short-wave (long-
 125 wave) flux minus the clear-sky short-wave (long-wave) flux.

126 Estimates of the models' ECS values were taken from *Forster et al.* [2013] and *Ge-*
 127 *offroy et al.* [2013]; except for the GFDL-CM3 and GFDL-ESM2G models, whose sen-
 128 sitivities were only estimated by *Forster et al.* [2013]; and the BNU-ESM model, whose
 129 sensitivity was only estimated by *Geoffroy et al.* [2013] (Supplementary Table 1). Com-
 130 parisons were also made with estimates by the same authors of the models' feedback pa-
 131 rameter β_F , where $ECS = F_{2xCO_2}/\beta_F$ and F_{2xCO_2} is the radiative forcing due to a dou-
 132 bling of CO₂ concentrations, and with estimates of the CRE-derived cloud feedback ($\beta_{F,cloud}$)
 133 from *Forster et al.* [2013].

134 Both studies estimated the β_F and ECS values from the 4xCO₂ experiments in
 135 the CMIP5 archive, but *Forster et al.* [2013] used the *Gregory et al.* [2004] method to
 136 estimate the values, whereas *Geoffroy et al.* [2013] estimated values as part of their it-
 137 erative fitting of an energy balance model. The two sets of estimates are highly corre-
 138 lated, with an r^2 value of approximately 0.95. The *Forster et al.* [2013] estimates will
 139 be referred to as $\beta_{F,1}$ and ECS_1 , and the *Geoffroy et al.* [2013] estimates as $\beta_{F,2}$ and ECS_2 .

140

2.2 ω decomposition

141

142

143

144

145

146

147

148

149

150

151

Following Bony and co-authors (*Bony et al.* [2004]; *Bony and Dufresne* [2005]), the data were binned according to their monthly-mean 500hPa vertical pressure velocity, ω , with a bin-size of 5hPa/day, as a way of isolating different regimes of the large-scale overturning circulation. Only tropical data were included in the binning, with the tropics defined as 30°S to 30°N, though the results are not qualitatively sensitive to the definition of the tropics or to the choice of bin size. After binning, annual-means were taken and the time-series were linearly de-trended to remove model drift, though note that some models have non-linear drift. Since the calculations are performed in frequency-space (see next section), they are not affected by regression dilution [*Proistosescu et al.*, 2018], and it was found that taking annual-means reduced the intermodel spread in the results of the regressions somewhat.

152

153

154

Tropical means can be taken by weighting the quantities in each bin by the probability density of that bin and then integrating over all bins. For instance, the tropical-mean surface temperature \bar{T} is

$$\bar{T}(t) = \int_{-\infty}^{+\infty} P(t, \omega) T(t, \omega) d\omega, \quad (1)$$

155

156

157

where $P(t, \omega)$ is the distribution of ω , $T(t, \omega)$ is the mean surface temperature in that bin and t is measured in years. The ensemble-median values of the time-averaged probability densities, $[P(\omega)]$, are shown in the left panel of Figure 1.

158

159

160

161

162

The variability of the tropical-mean CRE ($\bar{C}(t)'$, where $\bar{C}(t)' = \bar{C}(t) - [\bar{C}]$) can be decomposed into a “dynamic” component due to changes in the probability density of each bin ($P(t, \omega)'$), a “thermodynamic” component due to changes in the relationship between CRE and vertical velocity ($C(t, \omega)'$) and a non-linear component (*Bony et al.* [2004]; *Byrne and Schneider* [2018]):

$$\bar{C}'(t) = \int_{-\infty}^{+\infty} P(t, \omega)' [C(\omega)] d\omega + \int_{-\infty}^{+\infty} [P(\omega)] C(t, \omega)' d\omega + \int_{-\infty}^{+\infty} P(t, \omega)' C(t, \omega)' d\omega. \quad (2)$$

163

164

165

166

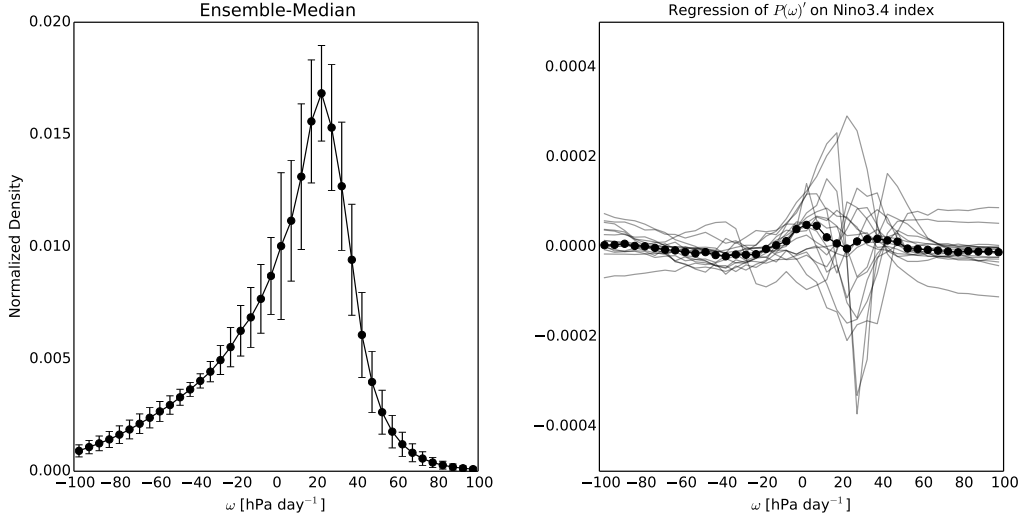
167

168

The dynamic term represents changes in the CRE due to large-scale circulation changes; for instance due to the re-organization of convection during ENSO events (note however that any dynamic effects that are decoupled from the ω velocities, such as lower tropospheric mixing, are not included in this term, and instead make up part of the thermodynamic term). The second term represents changes in cloud amount or in cloud radiative properties under fixed dynamic conditions, while the non-linear term, which is small,

169 represents co-variations of the dynamic and thermodynamic changes, and will be ignored
 170 hereafter.

171 The goal is to understand how different cloud-types are related to tropical-mean
 172 surface temperatures on ENSO time-scales and so the frequency-dependent regressions
 173 were performed between the tropical-mean surface temperature anomalies (\bar{T}') and the
 174 dynamic term, and between \bar{T}' and the thermodynamic term.



175 **Figure 1.** Left panel: Ensemble-median histogram of $[P(\omega)]$ for the 18 CMIP5 models an-
 176 alyzed in this study. The error bars show ± 1 standard deviation. Right panel: Regression of
 177 $P(t, \omega)'$ onto the Nino3.4 index for each of the models used in the study (light gray lines). The
 178 thick line with the markers shows the ensemble-median of the regressions.

179 2.3 Spectral analysis

180 The spectral analysis follows the same procedure as *Lutsko and Takahashi [2018]*,
 181 and is described in more detail in the Supplementary Text. The focus is on frequency-
 182 dependent regression co-efficients, which are calculated as

$$\tau(f) = \frac{C_{TR}(f)}{P_{TT}(f)}, \quad (3)$$

183 where f is frequency, P_{TT} is the power spectrum of global-mean surface temperature for
 184 a particular model and C_{TR} is the cross-spectrum of surface temperature with a partic-
 185 ular TOA flux R (the Fourier transform of the cross-correlation between T and R). Since

186 τ is complex it must be separated into its amplitude (a) and phase (ϕ):

$$a(f) = \frac{|C_{TR}(f)|}{P_{TT}(f)}, \quad (4)$$

187

$$\phi(f) = \tan^{-1} \left[\frac{\text{Im}\{C_{TR}(f)\}}{\text{Re}\{C_{TR}(f)\}} \right], \quad (5)$$

188 where $\tau = ae^{i\phi}$. $a \geq 0$ and values of a will be referred to as “amplitudes” as a short-
 189 hand for “amplitudes of the regression co-efficients”. The phase is always between -180°
 190 and 180° , with a phase of -180° being equivalent to a phase of 180° , and positive phases
 191 are taken to mean that the surface temperature leads the TOA flux.

192 To interpret the phases and amplitudes, note that if $\phi(f) = 0^\circ$ then an increase
 193 in $C(\omega)'$ corresponds to an increase in \bar{T}' , and the CRE from that bin acts as a nega-
 194 tive feedback on surface temperature. Conversely if $\phi(f) = 180^\circ$ then an increase in
 195 $C(\omega)'$ corresponds to a decrease in \bar{T}' , and the CRE from that bin acts as a positive feed-
 196 back on surface temperature. In both these cases, $a(\omega)$ can be interpreted as a feedback
 197 co-efficient. If $\phi(f) = \pm 90^\circ$ then one variable is proportional to the derivative of the
 198 other, with the sign of the relationship ambiguous. For instance, $dC(\omega)/dt = \bar{T}'$ and
 199 $d\bar{T}'/dt = -C(\omega)'$ will both produce a phase of $+90^\circ$. Physical reasoning must be used
 200 to differentiate between these two scenarios, with $a(\omega) = f^{-1}$ or f in the two cases, re-
 201 spectively. If the phase is not equal to 0° , $\pm 90^\circ$ or 180° then \bar{T}' and C' both have com-
 202 ponents which are linearly related (and so have a phase of 0° or $\pm 180^\circ$) and components
 203 which are in quadrature (and so have a phase of $\pm 90^\circ$).

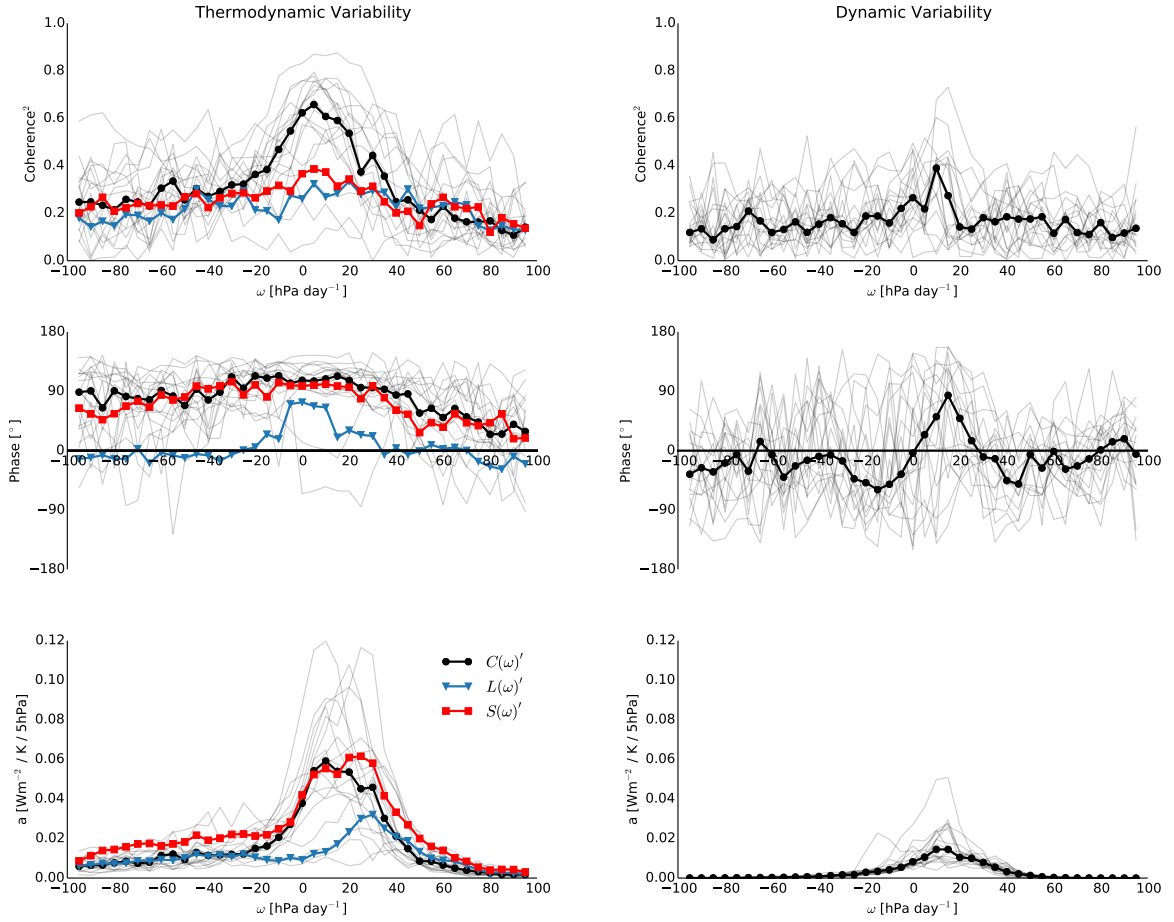
204 Finally, the squared coherence between T and R was also estimated:

$$\text{Coh}_{TR}^2(f) = \frac{|C_{TR}(f)|^2}{P_{TT}(f)P_{RR}(f)}, \quad (6)$$

205 which gives a sense of the robustness of the relationship between T and R at a partic-
 206 ular frequency.

215 **3 Regressions Between Thermodynamic Variability and Tropical-Mean** 216 **Surface Temperature**

217 The results of the regressions between $C(\omega)'$ (the binned net CRE) and \bar{T}' are sum-
 218 marized in the left panels of Figure 2. The values shown are averaged over the $1/2.5 \text{ years}^{-1}$
 219 to $1/3 \text{ years}^{-1}$ frequency band, since Lutsko and Takahashi demonstrated that this band
 220 can be used to predict the models' sensitivities, however the results are similar using a



207 **Figure 2.** Top left panel: squared-coherence between \bar{T}' and $C(\omega)'$ for ω between -
 208 100hPa/day and 100hPa/day, averaged over frequencies of $1/2.5 \text{ years}^{-1}$ to $1/3 \text{ years}^{-1}$. The
 209 individual models are in gray and the ensemble median is shown by the thick black line. The
 210 ensemble-median coherences for the regressions with the long-wave CRE ($L(\omega)'$) and the short-
 211 wave CRE ($S(\omega)'$) are shown in the thick blue and red lines, respectively. Middle left panel:
 212 same but for the phase between \bar{T}' and $C(\omega)'$. Positive phase means that surface temperature
 213 leads the TOA flux. Bottom left panel: same but the amplitudes between \bar{T}' and $C(\omega)'$ are
 214 shown. Right panels: same but for the regressions between $P(\omega)'$ and \bar{T}' .

221 wider range of frequencies in the ENSO range (Supplementary Figure 1). Individual model
 222 results are in light gray and the ensemble-median values are in black.

223 All three variables demonstrate the importance of the -10hPa/day to 25hPa/day
 224 bins for the relationship between tropical CRE and tropical surface temperatures. The
 225 coherence is generally low (0.2-0.4 in the ensemble-median), except at these velocities,

226 where it reaches values of more than 0.6 in the ensemble-median at 5hPa/day. Similarly,
 227 although the phase is close to $+90^\circ$ at all velocities, the intermodel spread is smallest
 228 for these velocities, with all but two of the models close to $+90^\circ$. The amplitudes are
 229 also largest for these regimes, with a maximum at 10hPa/day of about $0.06 \text{ Wm}^{-2}\text{K}^{-1}$
 230 (note that the values of a have been weighted by $[P(\omega)]$).

231 As in Lutsko and Takahashi, the 90° phase difference for the regions of weak as-
 232 cent and of weak-to-moderate subsidence can be interpreted as representing clouds am-
 233 plifying ENSO-induced surface temperature anomalies, with low cloud cover reduced dur-
 234 ing warm El Niño events, amplifying the warming of tropical-mean surface temperatures.
 235 Figure 3 supports this interpretation by showing lag-regressions between the tropical CRE
 236 averaged over the -10 to 25hPa/day bins and tropical-mean surface temperatures (top
 237 left panel); between the tropical CRE in these regions and the Nino3.4 index in the mod-
 238 els (top right panel); between the Nino3.4 index and tropical-mean surface temperatures
 239 (bottom left panel) and between the CRE and the cloud cover in these regions (bottom
 240 right panel). Note that linearly de-trended, monthly data were used to estimate these
 241 lag-regressions.

242 In line with the interpretation given above, the CRE is approximately in phase with
 243 the Nino3.4 index and these are anti-correlated, with a minimum correlation of around
 244 -0.4 in the ensemble-median. The CRE is also anti-correlated with tropical-mean tem-
 245 perature, but leads this by about four months in the ensemble-median. As expected, the
 246 Nino3.4 index is strongly correlated (co-efficient ~ 0.9) with tropical-mean surface tem-
 247 perature, and leads this by about three months in the ensemble-median. These relation-
 248 ships support the claim that the low cloud CRE quickly responds to ENSO-induced SST
 249 anomalies in the equatorial Pacific and then amplifies tropical-mean surface tempera-
 250 ture anomalies, which lag by several months. The CRE in these regions is highly cor-
 251 related with their cloud cover (bottom right panel), suggesting that tropical low cloud
 252 CRE variability is mainly due to changes in cloud cover, as opposed to changes in cloud
 253 thickness or depth.

254 To give a sense of the spatial structure of the ENSO-induced changes in tropical
 255 clouds, Supplemental Figure 2 shows regressions of the monthly estimated inversion strength
 256 (EIS, *Wood and Bretherton [2006]*), a proxy for low clouds and their thermodynamic en-
 257 vironment, onto the Nino3.4 index for six of the models used in this study. There are

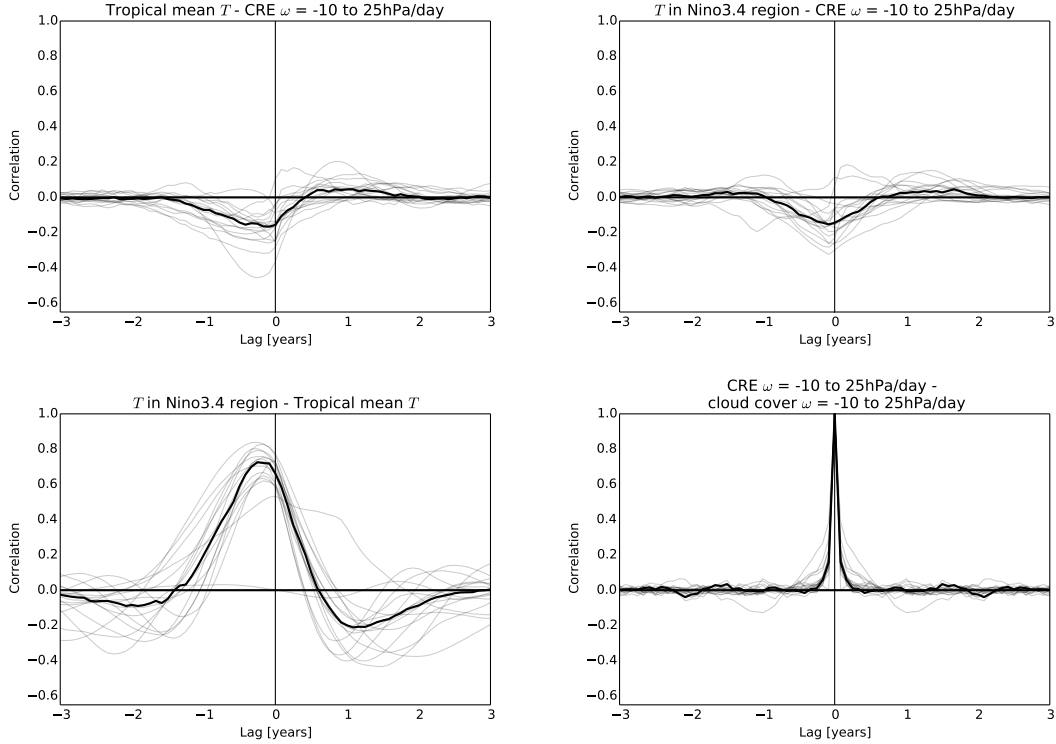
258 EIS changes throughout the tropics during ENSO events, and the panels also include boxes
 259 highlighting regions which have been identified as being important for low clouds [Wood,
 260 2006]. This reveals that the net low cloud CRE response results from a cancellation be-
 261 tween some regions with increases in low clouds and other regions with decreases, though
 262 the net effect is always for a reduction in low cloud cover. Understanding the differences
 263 between these regions and comparing how they behave in models and in observations is
 264 beyond the scope of this article, but will be required to fully understand the relation-
 265 ship between clouds and ENSO events.

266 The blue and red lines in Figure 2 show the results for the regressions with the long-
 267 wave and short-wave CREs ($L(\omega)'$ and $S(\omega)'$, respectively) with only the ensemble-median
 268 values shown for clarity. The regressions for $S(\omega)'$ generally resemble the $C(\omega)'$ regres-
 269 sions: the phase is always near 90° and the values of a are very similar, though they peak
 270 at about 30hPa/day instead of at 10hPa/day. The coherence is weaker than for the net
 271 CRE, with a maximum of about 0.5 at 5hPa/day. *Zelinka et al.* [2016] showed that low
 272 cloud cover is better correlated with net CRE than with short-wave CRE (which includes
 273 the CRE of high clouds), explaining the weaker coherence for $S(\omega)'$.

274 In contrast, there is little resemblance between the long-wave regressions and the
 275 net CRE regressions. The phase is always close to zero, except for a few values at ve-
 276 locities close to 0hPa/day when it approaches $+90^\circ$. There is a small peak in the am-
 277 plitudes at about 30hPa/day, but otherwise the amplitudes are small, while the coher-
 278 ence is weak for all bins. This peak in regions of strong subsidence is unexpected, since
 279 these regions are dominated by low clouds, which have a weak long-wave effect (*Bony*
 280 *et al.* [2004]), and the long-wave amplitudes appear to actually cancel the short-wave am-
 281 plitudes somewhat, so that the amplitudes for the net CRE are largest in regions of rel-
 282 atively weak subsidence.

283 In the ensemble-median, the longwave CRE is roughly in phase with \bar{T}' in these
 284 regions of strong subsidence, suggesting that it is acting as a negative feedback on tem-
 285 perature variability. But this is the result of cancellation between a wide spread in phases
 286 across the individual models (Supplementary Figure 3), making it difficult to interpret
 287 the reason for this peak. Lag correlations are also inconclusive, as the correlation between
 288 the low cloud long-wave CRE and tropical-mean surface temperature is very weak (not

289 shown). Clarifying the effect of the long-wave CRE of low clouds on surface tempera-
 290 ture variability will require focused modelling work.



291 **Figure 3.** Top left panel: lag correlations between tropical-mean surface temperature (R)
 292 and tropical CRE averaged over -10hPa/day to 25hPa/day . Positive lag means that temperature
 293 leads the CRE. The individual models are in gray and the ensemble median is shown by the thick
 294 black line. Top right panel: same for the Nino3.4 index and tropical CRE in the same regions.
 295 Bottom left panel: same for the Nino3.4 index and tropical-mean temperatures. Positive lag
 296 means that the temperature leads the Nino3.4 index. Bottom right panel: same for tropical CRE
 297 and tropical cloud cover in th same regions. Positive lag means the cloud cover leads the CRE.
 298 The Nino3.4 index was calculated by averaging SSTs in the Nino3.4 box (120°W - 170°W and 5°S -
 299 5°N), removing the mean and dividing by the standard deviation, and the lag correlations used
 300 de-seasonalized and de-trended monthly data from the models.

301 **4 Regressions Between Dynamic Variability and Tropical-Mean Sur-**
 302 **face Temperature**

303 Figure 3 repeats Figure 2, but for the regressions between $P(\omega)'$ and \bar{T}' . The re-
 304 lationship between these is weak, as the coherence and amplitude are both low at almost

305 all frequencies and there is much intermodel spread in the coherence and the phase. There
 306 is a weak peak in the amplitudes and in the coherence at about 10hPa/day, however, and
 307 the phase is close to 90° in the ensemble median at 10hPa/day. So although the dynamic
 308 variability is in general not an important component of the relationship between cloud
 309 fluxes and surface temperature variability on ENSO time-scales, it may play a role in
 310 regions of weak subsidence.

311 The minor role of dynamics in driving CRE variability is partly explained by the
 312 right panel of Figure 1, which shows the regressions of $P(\omega)'$ onto the Nino3.4 index for
 313 each model. The regressions exhibit very different behaviors across the models: in some
 314 $P(\omega)'$ is enhanced between about 0 and 40hPa/day and reduced everywhere else, while
 315 in others there is a shift in the distribution, as $P(\omega)'$ is reduced in regions of weak sub-
 316 sidence and enhanced in regions of strong subsidence. In all of the models, however, the
 317 largest values of the projections are only 1-5% of the climatological values of $[P(\omega)]$. So
 318 although there may be considerable re-organization of the convection in space during ENSO
 319 events, the relative fractions of the different regimes do not exhibit large temporal vari-
 320 ations in the models.

321 Another reason for the small role of dynamics is the roughly linear relationship be-
 322 tween CRE and ω : if this relationship were perfectly linear then, over a large enough re-
 323 gion, any reorganisation of the circulation that conserved mass would not change the CRE
 324 (*Wyant et al. [2006]; Byrne and Schneider [2018]*).

325 5 Comparing with Climate Sensitivity Estimates

326 As in Lutsko and Takahashi, the amplitudes can be thought of as frequency-dependent
 327 internal variability sensitivities, and so regressing them against the models' climate sen-
 328 sitivities is a way of investigating whether the models' internal variability is correlated
 329 with their sensitivities to external forcing. This is shown in Figure 4, which plots the r^2
 330 values for correlations between the amplitudes for $C(\omega)'$, averaged over the 1/2.5 to 1/3
 331 years⁻¹ frequency band, and the estimates of the models' β_F and ECS values.

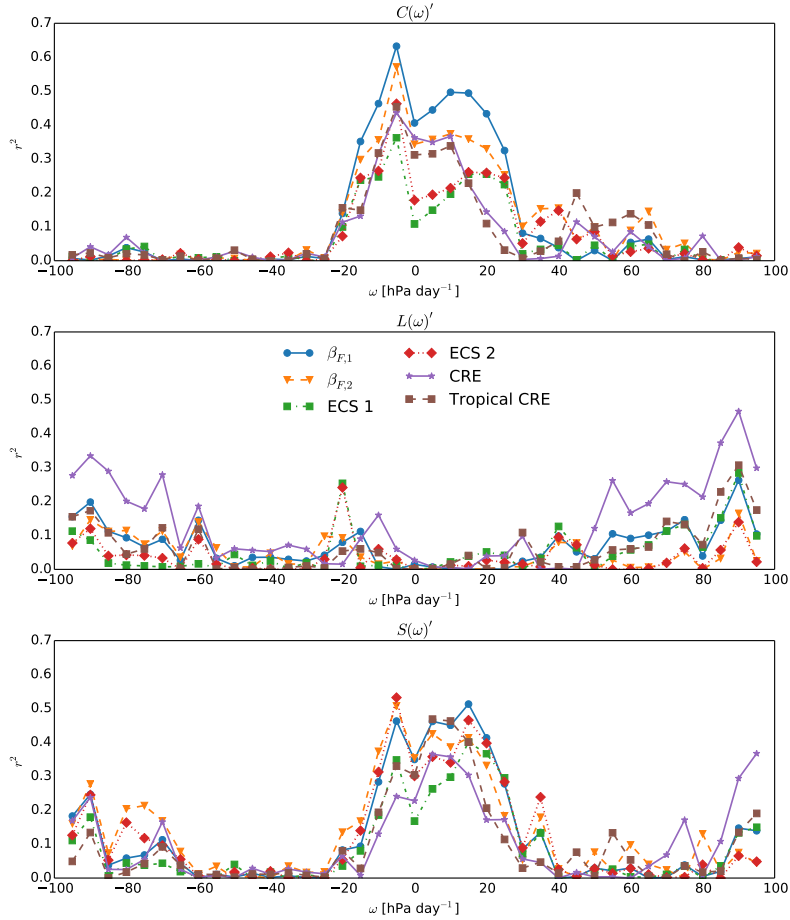
332 The strongest correlations are again in the -10hPa/day to 25hPa/day bins, with
 333 r^2 values of up to 0.6, and are weaker with the *ECS* estimates than with the β_F esti-
 334 mates. Decomposing into the short-wave and long-wave components demonstrates that
 335 most of this correlation comes from the short-wave (bottom panel of Figure 4), though

336 adding the long-wave improves the relationship somewhat [Zelinka *et al.*, 2016]. Plot-
 337 ting the values of $a(f, \omega)$, averaged over the -15 to 25hPa/day bins, against the sensi-
 338 tivity estimates shows that models with larger values of a have larger climate sensitiv-
 339 ities (smaller values of β_F , Supplementary Figure 4). That is, models in which clouds
 340 in regions of weak subsidence and weak ascent amplify tropical mean surface temper-
 341 ature variability more strongly on ENSO time-scales are more sensitive to external forc-
 342 ings. Intuitively, this is what we would expect: models which experience a larger reduc-
 343 tion in low clouds when tropical surface temperatures warm have larger climate sensi-
 344 tivities.

345 Similar results are obtained when the correlations are performed with the $\beta_{F,cloud}$
 346 estimates (purple lines in Figure 4) and estimates of the tropical-mean CRE feedback
 347 (brown lines in Figure 4, these are calculated using the same procedure as Forster *et al.*
 348 [2013] but only using tropical CRE values). However, the correlations are better for the
 349 estimates of the total feedback than for the estimates of the CRE feedback, which sug-
 350 gests that the highest r^2 values for the total feedback may be somewhat fortuitous. The
 351 CRE feedback estimates also do not account for the effect cloud masking, which may af-
 352 fect the CRE feedback and the regression co-efficients differently, and may cause the re-
 353 gression co-efficients to be more strongly correlated with the total feedbacks. The am-
 354 plitudes from the regressions with $P(\omega)'$ are not well correlated with the sensitivity es-
 355 timates (Supplementary Figure 5), as expected from the previous section.

361 6 Conclusion

362 The results presented here demonstrate that the relationship between tropical-mean
 363 surface temperature variability and tropical CRE on ENSO time-scales is dominated by
 364 the thermodynamic variability of clouds in regions of weak ascent and weak-to-moderate
 365 subsidence ($\omega \sim -10$ to 30hPa/day). This variability is 90° out of phase with surface
 366 temperature, and amplifies ENSO-induced surface temperature variability through re-
 367 ductions (enhancements) of low cloud cover during warm (cold) El Niño (La Niña) events
 368 (see also Klein *et al.* [1999]; Lau and Nath [2001]; Zhu *et al.* [2007]; Zhou *et al.* [2017]).
 369 A caveat to this picture is that the long-wave CRE of clouds in regions of strong sub-
 370 sidence (≥ 20 hPa/day) partly cancels these clouds' short-wave CRE, so that the net CRE
 371 in these regions has a smaller effect on surface temperature variability than clouds in re-
 372 gions of weaker descent. It is difficult to determine why the long-wave CRE in regions



356 **Figure 4.** Top panel: r^2 values for regressions between the four sets of sensitivity estimates,
 357 the estimates of the CRE feedback and the estimates of the tropical CRE feedback, and the am-
 358 plitudes, averaged over frequencies of $1/2.5 \text{ years}^{-1}$ to $1/3 \text{ years}^{-1}$, for the regressions between
 359 \bar{T}' and $C(\omega)'$. Middle panel: same for the regressions between \bar{T}' and $L(\omega)'$. Bottom panel: same
 360 for the regressions between \bar{T}' and $S(\omega)'$.

373 of strong subsidence has this effect because of the large intermodel spread in the phase,
 374 though it is worth noting that reductions in low cloud cover are often associated with
 375 an increase in the flux of water vapor from the boundary layer to the free atmosphere,
 376 which promotes the formation of mid/high clouds. In general CRE variability due to changes
 377 in the large-scale dynamics during ENSO events does not impact surface temperature
 378 variability, despite the substantial re-organization of convection in space during ENSO
 379 events, but it does seem to play a minor role in regions of weak subsidence ($\sim 10 \text{ hPa/day}$).

380 The frequency-dependent regression coefficients for the regressions between the net
381 CRE in these regions and tropical-mean surface temperatures are well correlated ($r^2 >$
382 0.6) across models with the models' sensitivities (Figure 4), with larger regression co-
383 efficients corresponding to models with larger climate sensitivities (Supplementary Fig-
384 ure 4). In other words, models which experience larger reductions (enhancements) of low
385 cloud cover during warm (cold) El Niño (La Niña) events have larger ECS values. This
386 constitutes a stricter emergent constraint than that proposed by *Lutsko and Takahashi*
387 [2018], as it depends on the CRE in particular dynamical regimes of the tropics, rather
388 than on the global-mean CRE, and agrees with the analysis by *Vial et al.* [2013], who
389 showed that regions of weak ascent and weak-to-moderate subsidence ($\omega = -10$ to 30hPa/day)
390 are largely responsible for the spread in ECS values in the CMIP5 models. A caveat is
391 that it has been shown previously that O(100 years) of data are needed to accurately
392 estimate ENSO spectra (*Wittenberg* [2009]; *Lutsko and Takahashi* [2018]), and so the
393 emergent constraint developed here is of limited practical use for the near-term.

394 These results add to our picture of how clouds influence surface temperature vari-
395 ability on ENSO time-scales and also to the growing body of literature showing that, de-
396 spite substantial differences in the patterns of tropical cloud changes during ENSO events
397 and in response to increased CO₂ concentrations, there is a strong relationship across
398 models between the CREs resulting from these cloud changes (e.g., *Zhou et al.* [2015];
399 *Brient and Schneider* [2016]; *Colman and Hanson* [2017]; *Lutsko and Takahashi* [2018]).
400 By focusing on the 1/2.5 to 1/3 years⁻¹ frequency band, this study clearly demonstrates
401 that this relationship comes from ENSO-induced cloud changes, while the decomposi-
402 tion of the fields into ω bins allows the key cloud regimes responsible for this relation-
403 ship to be identified. Future work involving focused modelling work as well as observa-
404 tional investigations are required to further understand how changes in CRE in regions
405 of weak ascent and moderate-to-weak subsidence influence tropical surface temperature
406 anomalies on ENSO frequencies, and how these changes relate to the CRE feedbacks seen
407 in climate change experiments.

408 **Acknowledgments**

409 I thank Max Popp, Cristian Proistosescu, Mike Byrne and Paul O'Gorman for helpful
410 conversations and comments on earlier versions of this manuscript, and two anonymous
411 reviewers for constructive comments, which improved the manuscript significantly. I also

412 thank the NSF for supporting me through grant AGS-1623218, “Collaborative Research:
413 Using a Hierarchy of Models to Constrain the Temperature Dependence of Climate Sen-
414 sitivity”. The CMIP5 data can be accessed at https://cmip.llnl.gov/cmip5/data_portal.html
415 and the scripts used in this analysis are available at https://github.com/nicklutsko/CMIP5_ENSO/.

416 References

417 Andrews, T., and M. J. Webb (2018), The dependence of global cloud and lapse rate
418 feedbacks on the spatial structure of tropical pacific warming, *Journal of Climate*,
419 *31*(7), 641–654.

420 Andrews, T., J. M. Gregory, and M. J. Webb (2015), The dependence of radiative
421 forcing and feedback on evolving patterns of surface temperature change in cli-
422 mate models., *Journal of Climate*, *28*(2), 1630–1648.

423 Bony, S., and J. L. Dufresne (2005), Marine boundary layer clouds at the heart of
424 tropical cloud feedback uncertainties in climate models., *Geophysical Research*
425 *Letters*, *32*(6), L20,806.

426 Bony, S., K. M. Lau, and Y. C. Sud (1997), Sea surface temperature and large-scale
427 circulation influences on tropical greenhouse effect and cloud radiative forcing.,
428 *Journal of Climate*, *10*(6), 2055–2077.

429 Bony, S., J. L. Dufresne, H. L. Treut, J. J. Morcrette, and C. Senior (2004), On
430 dynamic and thermodynamic components of cloud changes, *Climate Dynamics*,
431 *22*(6), 71–86.

432 Brient, F., and T. Schneider (2016), Constraints on Climate Sensitivity from Space-
433 Based Measurements of Low-Cloud Reflection., *Journal of Climate*, *29*(8), 5821–
434 5835.

435 Byrne, M. P., and T. Schneider (2018), Atmospheric dynamics feedback: Concept,
436 simulations and climate implications., *Journal of Climate*, p. Accepted.

437 Chiang, J. C. H., and A. H. Sobel (2002), Tropical tropospheric temperature varia-
438 tions caused by enso and their influence on the remote tropical climate, *Journal of*
439 *Climate*, *15*(9), 2616–2631.

440 Colman, R. A., and L. I. Hanson (2017), On the relative strength of radiative feed-
441 backs under climate variability and change., *Climate Dynamics*, *40*(1), 1–15.

442 Forster, P. M., T. Andrews, P. Good, J. M. Gregory, L. S. Jackson, and M. Zelinka
443 (2013), Evaluating adjusted forcing and model spread for historical and future

- 444 scenarios in the cmip5 generation of climate models, *Journal of Geophysical Re-*
445 *search: Atmospheres*, *118*, 1139–1150.
- 446 Geoffroy, O., D. Saint-Martin, G. Bellon, A. Voltaire, D. J. L. Olivie, and S. Tyteca
447 (2013), Transient climate response in a two-layer energy-balance model. part ii:
448 Representation of the efficacy of deep-ocean heat uptake and validation for cmip5
449 aogcms, *Journal of Climate*, *26*(6), 1859–1876.
- 450 Gregory, J. M., W. J. Ingram, M. A. Palmer, G. S. Jones, P. A. Stott, R. B. Thorpe,
451 J. A. Lowe, T. C. Johns, and K. D. Williams (2004), A new method for diagnos-
452 ing radiative forcing and climate sensitivity, *Geophysical Research Letters*, *31*,
453 L03205.
- 454 Klein, S. A., and D. L. Hartmann (1993), The seasonal cycle of low stratiform
455 clouds, *Journal of Climate*, *6*(6), 1587–1606.
- 456 Klein, S. A., B. J. Soden, and N.-C. Lau (1999), Remote sea surface temperature
457 variations during enso: Evidence for a tropical atmospheric bridge, *Journal of*
458 *Climate*, *12*(6), 917–932.
- 459 Lau, N.-C., and M. J. Nath (2001), Impact of enso on sst variability in the north
460 pacific and north atlantic: Seasonal dependence and role of extratropical seaair
461 coupling, *Journal of Climate*, *14*(7), 2846–2866.
- 462 Lloyd, J., E. Guilyardi, and H. Weller (2012), The role of atmosphere feedbacks dur-
463 ing enso in the cmip3 models. part iii: The shortwave flux feedback, *Journal of*
464 *Climate*, *25*(6), 4275–4293.
- 465 Lutsko, N. J., and K. Takahashi (2018), What can the internal variability of cmip5
466 models tell us about their climate sensitivity?, *Journal of Climate*, *31*(13), 5051–
467 5069.
- 468 MacMynowski, D. G., H. J., Shin, and K. Caldeira (2011), The frequency response
469 of temperature and precipitation in a climate model, *Geophysical Research Letters*,
470 *38*(23), 2011GL16711.
- 471 Park, S., and C. B. Leovy (2004), Marine low-cloud anomalies associated with enso,
472 *Journal of Climate*, *17*(6), 3448–3469.
- 473 Proistosescu, C., A. Donohoe, K. C., Amour, G. H., Roe, M. F., Stuecker, and C. M.
474 Bitz (2018) Radiative feedbacks from stochastic variability in surface temperature
475 and radiative imbalance, *Geophysical Research Letters*, *45*, 5082–5094.

- 476 Radel, G., T. Mauritsen, B. Stevens, D. Dommenges, D. Matei, K. Bellomo, and
477 A. Clement (2016), Amplification of El Nio by cloud longwave coupling to atmo-
478 spheric circulation, *Nature Geoscience*, *9*(106), 106–111.
- 479 Silvers, L. G., D. Paynter, and M. Zhao (2018), The diversity of cloud responses
480 to twentieth century sea surface temperatures. *Geophysical Research Letters*, *45*,
481 391–400.
- 482 A. H. Sobel and C. S. Bretherton (2002), Modeling Tropical Precipitation in a Single
483 Column, *Journal of Climate*, *13*(9), 4378–4392.
- 484 Vial J., J.-L. Dufresne, and S. Bony (2013), On the interpretation of inter-model
485 spread in cmip5 climate sensitivity estimates., *Climate Dynamics*, *41*(1), 3339–
486 3362.
- 487 Wittenberg, A. T. (2009), Are historical records sufficient to constrain ENSO simu-
488 lations? *Geophysical Research Letters*, *36*, 2011GL12702.
- 489 Wood, R. and C. S. Bretherton (2006), On the Relationship between Stratiform
490 Low Cloud Cover and Lower-Tropospheric Stability, *Journal of Climate*, *19*(12),
491 6425–6432.
- 492 Wood, R. (2006), Review: Stratocumulus Clouds, *Monthly Weather Review*, *134*(12),
493 2333–2423.
- 494 Wyant, M. C., C. S. Bretherton, J. T., Bacmeister, J. T., Kiehl, I. M., Held, M.,
495 Zhao, S. A. Klein, and B. J., Soden (2006), A comparison of low-latitude cloud
496 properties and their response to climate change in three AGCMs sorted into
497 regimes using mid-tropospheric vertical velocity., *Climate Dynamics*, *27*(23),
498 261–279.
- 499 Zelinka, M. D., C., Zhou, and S. A. Klein (2015), Insights from a refined de-
500 composition of cloud feedbacks *Geophysical Research Letters*, *42* 9259–9269,
501 2016GL069917.
- 502 Zhao, M., J. C. Golaz, I. M., Held, V. Ramaswamy, S. J. Lin, P. Ginoux, B.
503 Wyman, L. J. Donner, D. Paynter and H. Guo (2016), Uncertainty in model
504 climate sensitivity traced to representations of cumulus precipitation microphysics,
505 *Journal of Climate*, *29*(23), 543–560.
- 506 Zhou, C., M. D. Zelinka, A. E. Dessler, and S. A. Klein (2015), The relationship
507 between interannual and long-term cloud feedbacks, *Geophysical Research Letters*,
508 *42*(23), 10,463–10,469, 2015GL066698.

509 Zhou, C., M. D. Zelinka, and S. A. Klein (2017), Analyzing the dependence of global
510 cloud feedback on the spatial pattern of sea surface temperature change with a
511 green's function approach, *Journal of Advances in Modeling Earth Systems*, 9(23),
512 2174–2189.

513 Zhu, P., J. J. Hack, J. T. Kiehl, and C. S. Bretherton (2007), Climate sensitivity of
514 tropical and subtropical marine low cloud amount to enso and global warming due
515 to doubled co₂, *Journal of Geophysical Research*, 112(1), D17,108.